5-2020

Determining the Rotational and Orbital Velocities of Objects in the Solar System

Mark Jones

Determining the Rotational and Orbital Velocities of Objects in the Solar System

Mark Jones

April 22, 2020

Abstract

Astronomers have been observing the night sky for many centuries to establish a better understanding for our universe and solar system. As part of their observations, astronomers characterize celestial bodies by fundamental properties such as mass, motion, and composition in order to provide further insight about the objects in question. As technology and science have evolved, the methods for measuring these properties have become more precise and accurate. One such methodology is known as spectroscopy, and it is a significant tool for observational astronomy. In this paper, we shall describe how we used astronomical spectroscopy to determine orbital and rotational velocities for various objects in our solar system. This method was implemented specifically using the facilities of the Harry D. Powell Observatory on the campus of East Tennessee State University.

Contents

1 Introduction

The campus of East Tennessee State University(ETSU) is home to the Harry D. Powell Observatory. The observatory is maintained and administered by the Department of Physics and Astronomy at ETSU. Currently, students mainly use the observatory for astronomy labs, but there is also a course offered known as Variable Stars which focuses on independent astronomy research. Requirements for this course involve students observing a single variable star for multiple nights over the course of a semester, and then performing photometry on their retrieved images at the end. Although there is some formal instruction with the course, it still allows students to become familiar with telescope operation and astronomical programs in an independent setting.

Recently, the Department of Physics and Astronomy purchased a new astronomical instrument for the observatory– a spectrograph. With this new instrument, there is a pedagogical potential for a new course involving undergraduate research utilizing astronomical spectroscopy, or perhaps an inclusion of the instrument in the already existing course Variable Stars. In this work, we intend to substantiate the potential use of the spectrograph for student research by determining values for the rotational velocities of Jupiter, Saturn, and Saturn's rings, and the orbital velocities for two of the Galilean Moons.

2 Background

2.1 Planetary Motion

The planets and stars have always been spectacles of the night sky, and naturally, individuals throughout history became intrigued by what they saw above, leading them to try and further rationalize their sights through philosophy and science. For an extended period of time, there was much debate over the model of our solar system, and specifically the motion of the planets. In the ancient times, before telescopes and other modern-day astronomical instruments, the naked eye was the best tool for observation. The geocentric model of Claudius Ptolemy (c. 100 – c. 170) was the first complete attempt at describing the motion of the planets[3]. Although physically incorrect, it survived for some 1500 years. It was not until the time of Johannes Kepler (1571-1630) that planetary motion was universally formalized with mathematical equations, which later became known as Kepler's Laws of Planetary Motion. However, Kepler was not the first to publish a model describing the Earth orbiting the Sun. One of Kepler's predecessors, Nicolaus Copernicus (1473-1543), was

the first to push the idea of a heliocentric universe although his model lacked the precision and predictive power of Kepler's Laws[3]. Besides Kepler and Copernicus, another major contribution for understanding planetary motion came from Giovanni Cassini (1625-1712), who was the first to precisely measure the distance from Earth to Mars. Following Kepler's Laws, Cassini then used the Earth-Mars distance to determine the size of the solar system [3]. From these discoveries and many others, the understanding for the mechanics of our solar system was molded into a deep mathematical formulation, although there was still more knowledge to be gained.

Although better known for his laws governing motion and gravity, Isaac Newton (1643-1727) also explored the nature of light and colors. He was the first to describe how a prism could refract light from the Sun such that it would separate into its component colors. The colors had different degrees of refraction according to wavelength[5], resulting in a band of light known as a spectrum. It was over a century before this concept was applied to astronomy to investigate the light from planets and stars more extensively. The first detailed astronomical spectrum to be observed was that of the Sun by Joseph von Fraunhofer (1787-1826)[3]. Around this same time, experiments in laboratories made profound progress in the understanding of the spectrum of visible light from matter. This led to the creation of an entirely new method for investigating the properties of matter and the universe itself.

2.2 Spectroscopy

Matter is ubiquitous in our universe, and all of it is comprised of a fundamental entity known as the atom. By better understanding atoms and their interactions, astronomers can make inductive conclusions about the matter found in the rest of the universe. The concept of spectroscopy is rooted in atomic interaction, thus making it a significant tool when studying any type of celestial object made of matter such as galaxies, stars, and planets.

Light can be described as a quantum of energy (a particle model), the photon, or as a continuous electromagnetic wave. In either model, it is the energy transported by the light that is of most interest. When describing light as a wave, one must specify its frequency or wavelength value. By using either one of these values, its energy can be quantified by the following formula[6]

$$E = hf = \frac{hc}{\lambda} \tag{1}$$

where $f \equiv$ frequency, $c \equiv$ speed of light, $\lambda \equiv$ wavelength, and h is Planck's constant. The electromagnetic spectrum classifies every type of electromagnetic wave

in our universe with a specific frequency value and associated wavelength value. In spectroscopy, understanding this classification is critical for analysis.

The key characteristic in describing the state of an atom is energy. In a simplified view of quantum mechanics, the amount of energy, or energy level, in any given atom is quantified by a discrete scaling rather than a continuous one, meaning there are specific energy levels at which the atom is allowed to exist (e.g. E_1, E_2 are allowed but not $E_{1.345}$, where the subscript represents the energy level). Since these levels are discrete, there are very specific energy differences associated with transitioning between levels. From equation (1), this implies that there must be a specific frequency or wavelength value that corresponds to each energy transition, and therefore each specific energy difference of transitioning can be associated with a particular frequency or wavelength of electromagnetic radiation, and can be visually observed through the presence of "lines" in the light spectrum. The differences between spectral lines of corresponding emission and absorption spectra can be seen with respect to a given continuous spectrum in Figure 1[4]. The emission spectrum has a discrete set of specific bright spectral lines (emission of radiation from atomic electrons), whereas the absorption spectrum has a set of corresponding dark lines (absorption of radiation by atomic electrons) subtracted out from the continuous spectrum.

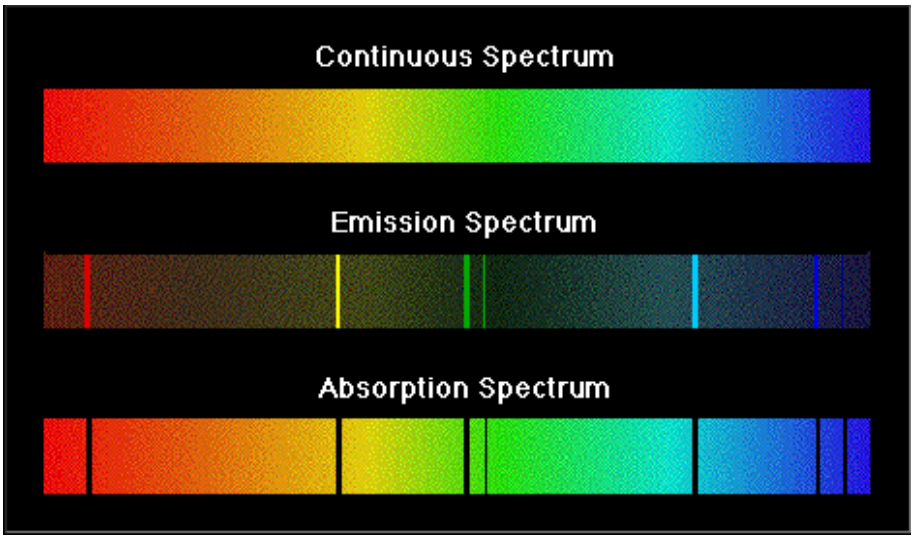

Figure 1: Different Types of Spectra

It is the analysis of spectral lines that is the prime focus of spectroscopic measurement in observational astronomy. With the entire spectrum of electromagnetic

radiation, spectroscopy provides a rigorous evaluation for determining physical quantities in celestial bodies. In particular for this work, spectral lines can be used to determine the motion of an object by applying the concept of a physical phenomenon known as the Doppler Shift.

2.3 Doppler Shift

The idea of a wave is quintessential to every field in physics. Waves can be used to describe light, sound, and even atomic particles. In the fields of cosmology and observational astronomy, electromagnetic and gravity waves are the only resource scientists have to study our universe. As one aspect of studying these types of waves, the Doppler Shift is essential for understanding the motions of objects that emit waves. This physical phenomenon occurs when a wave source and wave observer have some relative velocity with respect to each other along the line of sight between them. This relative velocity causes a distorted perception for observation of the wave's true properties, a 'shift' in wavelength or frequency of the wave. Observation of the shift allows one to determine velocity information or knowledge of velocities can allow one to correct for the shift in the observed spectrum.

Every observer has a set of coordinates described by a coordinate system, or rather, a reference frame . Consider a light source and observer to be at rest in the same reference frame. This source will emit light at a constant speed c with frequency f and wavelength λ. From equation (1), the speed of light can be expressed as the following

$$c = f\lambda \tag{2}$$

from which the observer can record the specific frequency f and wavelength λ for the light wave. Now consider the source of light to be moving at velocity V toward the observer with the same emitted frequency f and wavelength λ in the reference frame of the source. Since the source is moving at velocity V in the same direction as the emitted wave, the wavelength will be compressed by a factor of$(c - V)/f$ in the reference frame of the observer. Nevertheless, the light wave itself still moves at speed c regardless of the motion from another reference frame, so the observer will still record a speed c for the light. Recall that the wavelength and frequency of a wave are inversely proportional. Therefore, since the wavelength appears to be decreased, the observer will record a new frequency of the wave f' which appears to be increased from the original frequency. The general formula for f' can be expressed as the following[1]

$$f' = f\frac{1 \pm \frac{v}{c}}{1 \pm \frac{V}{c}} \tag{3}$$

where $v \equiv$ the velocity of the observer and the relative plus or minus sign depends upon the directions of velocities between the source and the observer. When an object has a positive shift in its velocity (i.e., towards the observer), the observed frequency is higher and the light is said to be "blue-shifted", and when a negative shift (i.e., away from the observer) it is said to be "red-shifted".

Equation (3) can be modified to solve for the velocity of the source, given the values of the other variables. Therefore, this general concept of the Doppler Shift can be used for calculating the velocities of any celestial body, specifically through the radial velocity method which will be discussed further in the next section. Note, this equation only holds true for objects moving at speeds much,much less than c. If an object is moving at a relativistic speed, or rather a speed which is close to c, then the laws of Special Relativity apply and equation (3) would be invalid. However, the solar system objects we are studying in this work move at non-relativistic speeds, thus equation (3) is valid for our calculations.

3 Methodology

Recall from the previous section that a reference frame is synonymous with a coordinate system. The importance of the coordinate system is such that one can describe quantities with not only magnitude, but also spatial direction. From this, we can describe vector quantities– those which have both a magnitude and direction– and we can dissolve vectors into components along the dimensional axes by using trigonometry and geometry. When considering the motion of planets and other celestial objects, it's important to understand one's reference frame in order to measure vector quantities, such as velocity and displacement.

Suppose a star is moving in some arbitrary direction in space, where our line of sight is an axis that runs directly between the star and us. The total velocity of the star might not necessarily be moving perfectly aligned with our line of sight, but there will be some component along our axis. This component of velocity along our line of sight is called the radial velocity[7], and the determination of such a quantity is heavily dependent upon the Doppler Shift due to light's behavior as a wave.

Hippolyte Fizeau(1819-1896) showed that a moving object's spectral lines would have a displacement that was directly proportional to the change in period (or frequency) with which they reached an observer[8]. In other words, the observed spectral line changes allowed one to measure the Doppler Shift in analysis of the spectrum, which is commonly referred to as the Doppler-Fizeau effect. The determination of radial velocity comes as a direct derivation from this effect which is expressed by the

following formula[7]

$$V_r = c \times \frac{\Delta\lambda_{obs}}{\lambda_{rest}} \tag{4}$$

where $c \equiv$ speed of light, $\Delta\lambda_{obs} \equiv$ displacement of the spectral line wavelength, and λ_{rest} is the known rest wavelength value of the spectral line.

For unresolved, point sources which emit light like stars, equation (4) can be used for calculating their radial velocity. However, our objects are resolved and rotating (the moon orbits can be considered similar to a rotation) and the spectra from our objects consists of reflected light from the Sun. Thus, we must make a "correction" to equation (4) to make it valid for our work. In regard to the rotation of a body (or moon orbit elongation), there will be one side of its spectrum that is coming towards us ("blue-shifted") and one side which is moving away ("red-shifted"). Because of this, we must account for the Doppler Shift twice, and thus multiply by a factor of 1/2. As a further matter, since the light which was observed for each object was reflected light, we must also account for the Doppler Shift twice *yet again* because the light was shifted upon absorption and again upon reflection requiring we multiply by another factor of 1/2. Thus, our total correction factor is 1/4 causing equation (4) to become

$$V_r = \frac{1}{4} \times c \times \frac{\Delta\lambda_{obs}}{\lambda_{rest}} \tag{5}$$

From equation (5), we are able to calculate the true radial velocity for our objects.

The terms "red-shift" and "blue-shift" come from the $\Delta\lambda_{obs}$ term as a reference to the color in the electromagnetic spectrum. When an object is red-shifted, it will have a longer wavelength and therefore be shifted towards the red side of the spectrum, as opposed to the blue-shift whose value will be shifted towards the blue side because it will have a shorter wavelength. An example of a red-shifted spectrum can be seen in Figure 2[7], where the all the spectral lines have been shifted toward the red side of the spectrum. For our work, we are not as concerned with the red or blue shift because it is rather arbitrary as to which spectrum or part of the spectrum is blue or red shifted. We are mainly interested in the total amount of shift to allow the use of equation (5) to find the radial velocity for each of our objects in question.

As previously discussed, velocity is a vector quantity, and we must consider its components appropriately in the reference frame of our observations. When considering the motion of Io and Callisto in particular, we must take into account how the motion of the Earth affects our observations as these occurred with the Earth at different orbital positions around the Sun. Luckily for us, there is a ginormous astronomical community heavily involved with computation. Within this community the Python programming language has integrated within it a package called

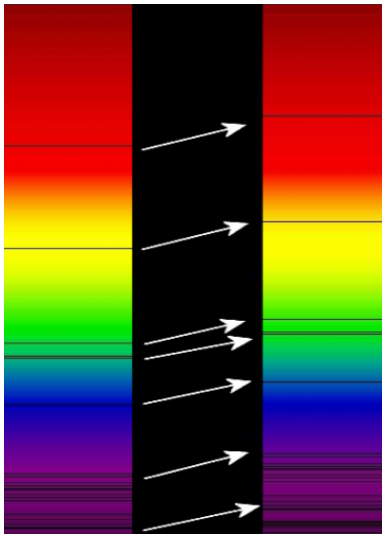

Figure 2: Red-shifted Spectrum

Astropy[1] for such specific astronomical computation. Using this package, we are able to calculate the value for the velocity correction from the Earth's space motions (known as the barycentric correction) in our spectra observations of Io and Callisto. Note, this correction was not applied to the spectra of Jupiter and Saturn as these spectra were acquired over just a span of a few minutes during a single night. Thus, the magnitude of the rotational Doppler shift we are interested in for those objects was not influenced by the Earth's motion although the actual wavelength values may have shown a slight shift from their rest wavelength values.

4 Procedure

We scheduled potential nights of observation to retrieve our spectra by using the Jupiter Ephemeris Generator 2.6[2]. Jupiter and Saturn required no specificity for planning an observation date because their rotational velocities could be measured from a single spectrum. However, observation of the Galilean Moons had to be more precisely timed in order to insure we obtained spectra at maximum elongation between the moon and Jupiter. It is at these points in their orbits when their velocities should be directed almost entirely along our line of sight from the Earth (either towards or away from us). A graphical display of the ephemeris generator output is

[1]https://www.astropy.org/

shown in Figure 3[2]. Several nights of observation were planned for each moon in

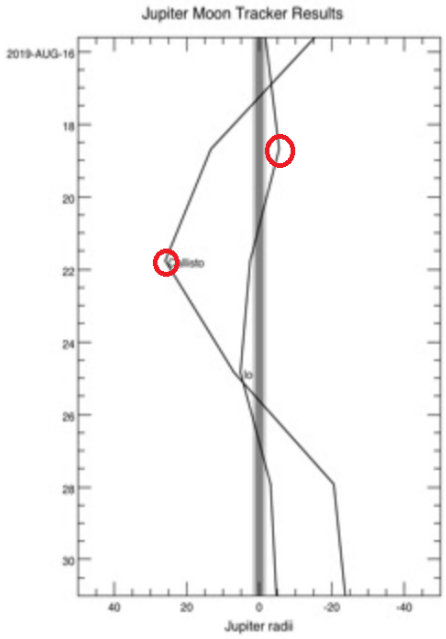

Figure 3: Ephemerides for Callisto and IO. Potential dates of observation at maximum elongation are circled for each moon

order to acquire spectra at the maximum elongation on both sides of the planet. The observations were obtained as near as possible to the exact time predicted by the generator program but could vary by an hour or more depending on the observing conditions. At the very minimum, two observations were required, one each from the opposite elongation positions so that a maximum shift in the spectral lines (one side of the orbit is blue-shifted, the other side red-shifted) would yield a $\Delta\lambda_{obs}$ term for equation (5).

All of our spectra were taken at the Harry D. Powell Observatory, located on the campus of East Tennessee State University. For a typical night of observations, we attempted to observe the objects near the time when they would transit (lie highest in the sky along the local meridian). For our spectra observations we used a Shelyak LHires III spectrograph with an SBIG Aluma 814 CCD camera for imaging the spectra. The spectrograph and camera were mounted at the focal plane of the observatory's Celestron C14 telescope. The telescope and instruments were remotely controlled from a warm room adjacent to the dome. Table 1 gives the specifications for the telescope, spectrograph, and camera while Figure 4 shows images of the setup.

Table 1: Instrument Specifications

Shelyak LHires III	• resolving power ∼17000 • 2400 lines/mm grating • Littrow optical design • 0.114 Å/px dispersion near H-alpha • 23 μm slit width
SBIG Aluma 814	• 9 megapixel chip • 3.69 micron square pixels • 3388 pixels x 2712 pixels • 14.6 mm x 12.8 mm • -50°C Max cooling temp
Celestron C14	• 355.5 mm aperture • 3910 mm focal length • f/11 focal ratio

Two computers were used in the control room. One to control the telescope and one to control the CCD camera. For the spectrograph we only had to turn on and off the calibration lamps (internally mounted in the spectrograph) through external switches. Maxim DL was the software program used to control the camera while TCSCOM was the program controlling the telescope on a computer dedicated to only that function. At the beginning of the night the CCD was cooled to -20°C (lower if ambient temperature allowed it) and allowed to stabilize to minimize thermal noise in the images. We also had a TV monitor screen to view live feed from the guide

Figure 4: From left to right– Telescope Dome, Control Room, Spectrograph and CCD

camera monitoring the slit entrance of the spectrograph. The telescope was manually guided with a hand control paddle to make tracking corrections to keep the object centered on the slit. In the TCSCOM program, we manually inputted the current time and date and thereafter selected the particular object we needed to observe. Once this was done, the telescope would then move automatically to a position that placed our object in the field of view of the finder telescope mounted on the side of the C14. If necessary, we manually adjusted the positioning of the telescope until the object appeared on the monitor screen with the slit in the control room. After the object was in the optimal position on the slit for acquiring spectra, we used Maxim DL to acquire spectra and the necessary calibration images with the spectrograph.

One important aspect about our spectrograph is that the grating position must be manually adjusted via an external micrometer for different ranges of wavelength. Thus, it is very inefficient to observe more than one part of the spectrum for a given observation and setting the grating position by hand is not highly accurate. As a result, we chose to observe at only one grating position and did not disturb the grating during the course of the observations reported here. We decided to observe the wavelength range from 6480 to 6630 angstroms (Å) because one of the most prominent solar absorption lines can be found there- the hydrogen alpha line– which will be the focus for our analysis.

In addition to obtaining images of the spectrum for each target object, a series of calibration images were needed to eliminate noise, normalize intensity measurements, and establish the correct wavelength scale for the spectra. These calibration images were bias, dark, and flat images to be used in calibrating the CCD performance and Neon lamp images to be used to calibrate the wavelength scale. A single exposure time for Io was 800 seconds in order to produce a reasonably strong signal to noise

ratio. An exposure time of 600 seconds was used for the other objects. Three such exposures would be taken and could later be stacked (co-added) to further improve the image statistics. The dark, flat, and lamp images were exposed as necessary (with dark images exposed for the same times as the light images) for their respective calibration purpose. Bias images have zero second exposures as they are simply a readout of the CCD image frame to establish the level of "read noise" for the camera. Multiple images of each calibration type were taken each night to be averaged in the calibration process to improve noise statistics.

The dark images represent a measurement of the "thermal" noise due to excitation of electrons in the semiconductor material of the CCD chip. Although cooling the chip minimizes such excitation, it does not eliminate it at the temperatures we used. Such noise increases with time of the exposure so dark images are exposed for the same time as the light images. The flat images require a uniform illumination of the CCD chip to measure the response of each individual pixel to the light falling upon it. This is difficult for the optical design of a spectrograph. We used two approaches for imaging them. One approach was done by turning on the flat lamp inside the spectrograph to illuminate the slit with a broad light source; the other was executed by placing an LED light flat-panel on top of the telescope tube to illuminate the entire optical path to the slit. For the most precise wavelength calibration, neon lamp images were taken both before and after images of the objects. The neon lamp exhibits emission lines of known wavelength which can be used to calibrate pixel location with wavelength for the spectra. Three bright emission lines were visible for the grating position used in our observations.

5 Analysis

5.1 Data Processing

The initial photometric calibration for all light images followed the standard procedure for CCD image reduction applying bias, dark, and flat images. Maxim DL was used to process the images in this way. Bias and dark images were median averaged for each night to create master images of each. These were then applied to the flat images which were then median averaged to create a master flat image. Each raw light image then had the master bias and dark images subtracted from it before being divided and normalized by the flat image. Finally, the calibrated images were then stacked to create a single spectrum image that was loaded into the spectra reduction program Basic Astronomical Spectroscopy Software (BASS)[9]. Figure 5 depicts what each calibration image typically looks like for a given night. The BASS

Figure 5: From left to right– Bias, Dark, Flat

program was then used to wavelength calibrate the images.

The first step was to correct the images for slant, tilt, and hot pixels. The slant and tilt corrections were made using the neon lamp lines. Given the complicated light path from the slit to the CCD, the spectrum image can be slightly distorted. The neon emission lines should ideally be straight and narrow, for example. That is not the case for the raw spectrum, however (see Figure 6). The slant correction adjusts the pixels horizontally to make the spectrum undeviating along the vertical, as shown in Figure 6. The tilt correction is similar to the slant correction, only it adjusts the pixels vertically to make the spectrum aligned along the horizontal. Finally, we had to correct for hot pixels in the image, which were caused by thermal anomalies in the semiconductor material of the CCD. This correction was done by averaging the pixels that were above a particular threshold value of intensity with the values of their nearest neighbors.

Once we had stacked spectra and neon calibration images corrected for slant, tilt, and hot pixels, our images looked like the following in Figures 7. Note, Saturn's rings are represented by the top and bottom bands on Saturn's spectrum, where the disk of Saturn is in the middle. Moreover, the images of Callisto and Io's spectra have two separate nights, one from each elongation in the orbit, stacked on top of one another to emphasize the shift in the hydrogen alpha line. We note also the slant of the hydrogen alpha line in the Io spectrum is not due to the rotation of Io. We suspect this is due to reflected light from Jupiter, but further investigation is needed to verify that as the source.

One interesting aspect about the spectra is the appearance of vertically straight telluric lines interspersed with the slanted solar lines. The telluric lines are straight because they come from the Earth's atmosphere, which is stationary in our reference frame, so therefore they are not affected by the Doppler Shift. However, the solar

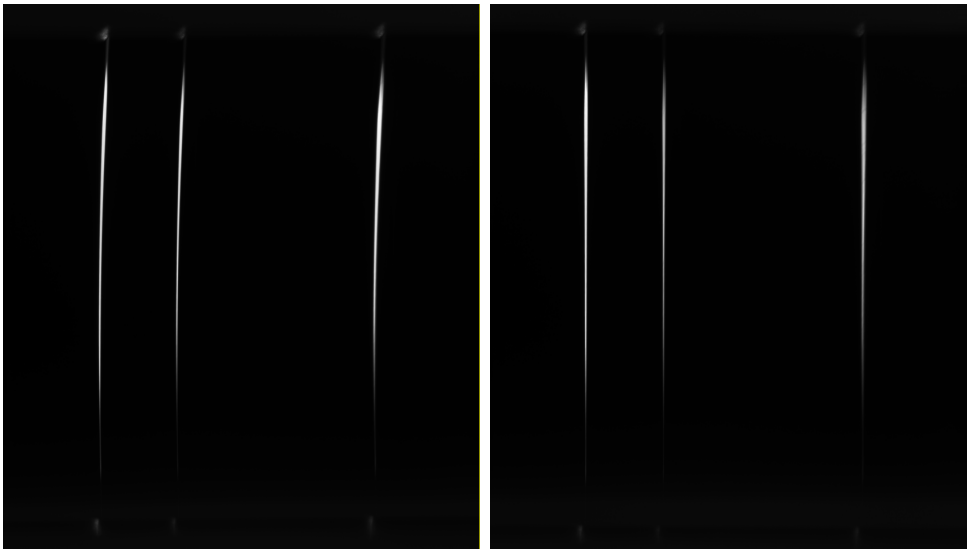

Figure 6: Neon emission spectrum near H-alpha, raw spectrum on the left showing distortion, spectrum corrected for slant and tilt on the right.

lines originate from reflected light by objects which are rotating in our reference frame, causing them to appear slanted in the spectrum. Since we are resolving the disk of the planets, both blue and red-shifted components are visible.

After we finished processing our images, the BASS program then uses the known wavelength values of the three spectral lines from the neon emission spectrum to calibrate the horizontal pixel scale in terms of wavelength; fitting the emission spectrum lines to their wavelengths and determining the linear dispersion in Angstroms/pixel for the spectra. Upon the above calibration, BASS creates a line graph which looks like the following in Figure 8 for a spectrum of Io. Both the neon emission lines (at bottom, in blue) and the absorption spectrum of Io (at top, in green) are shown. The horizontal axis is wavelength and the vertical axis is a relative intensity. If there is no calibration, the graph will have numerical pixel values on the horizontal axis instead of wavelength. From here, the x and y axis values could then be exported into a .xls file for further quantitative examination of the spectral lines. We repeated this process for the spectra of the objects for every night of observation for the vertical "bins" chosen from each spectrum as described below.

As described previously, the spectral line we considered for the Doppler shift calculations was the hydrogen alpha line with a rest wavelength of 6562.80 Å. This will be our value for λ_{rest} in equation (5). This line is the most prominent, the strongest in absorption, and the most easily identifiable in the spectra.

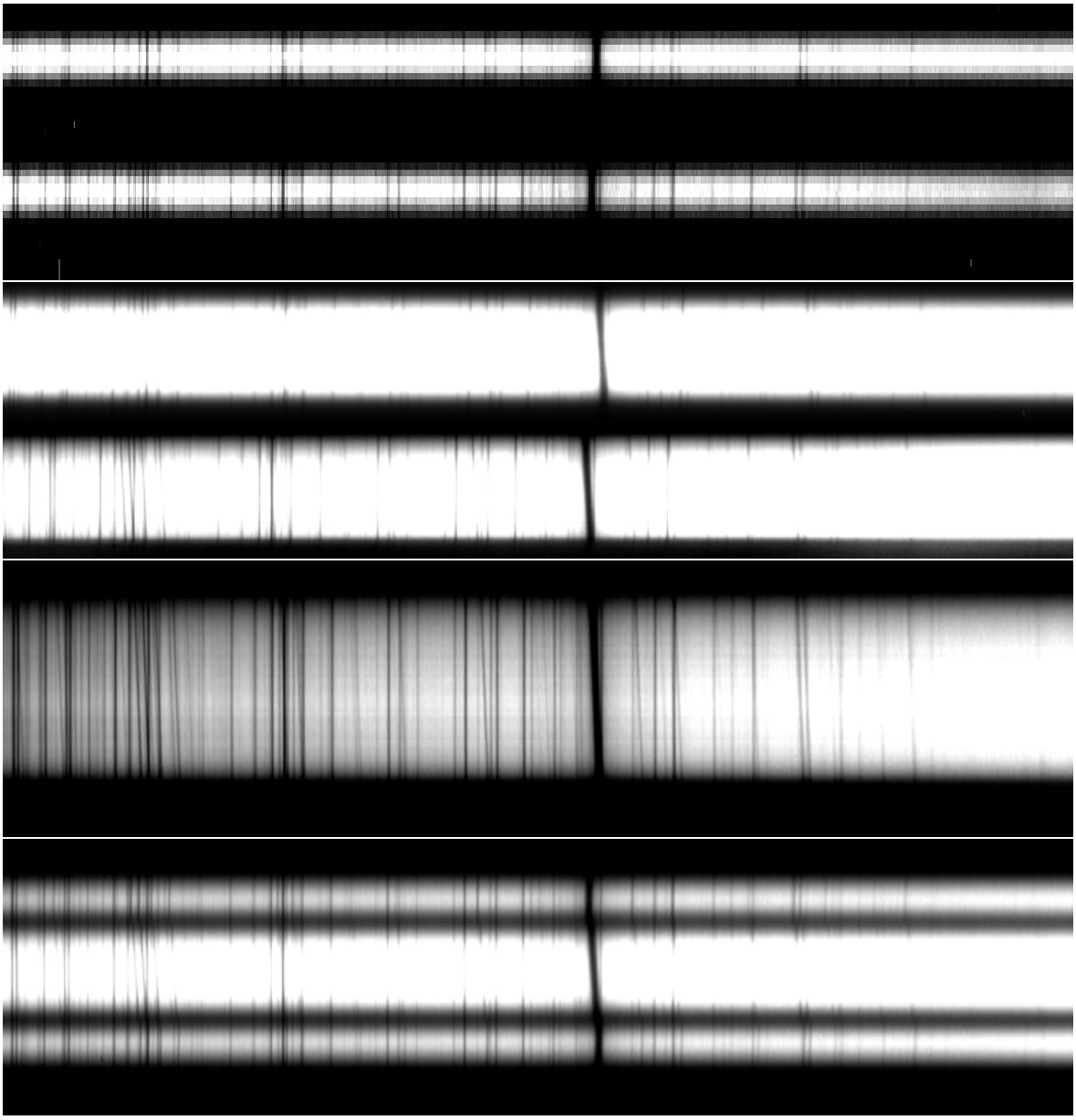

Figure 7: From top to bottom– Callisto, Io, Jupiter, Saturn Spectra

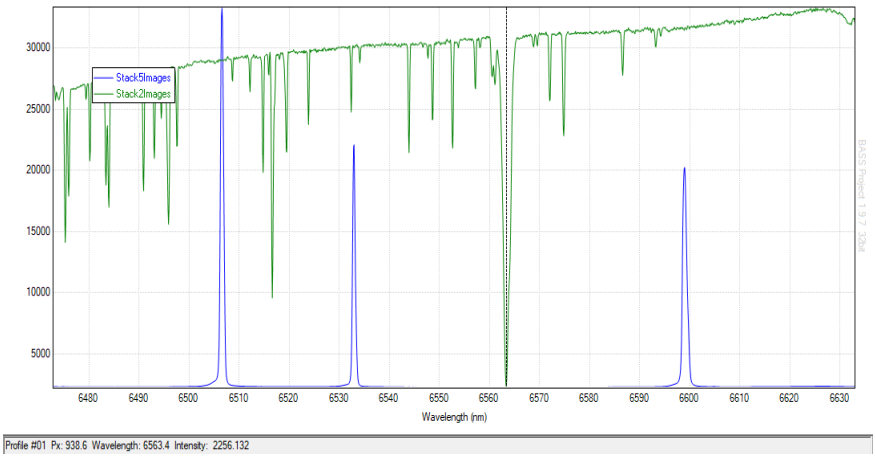

Figure 8: Wavelength calibrated spectrum for Io

For Jupiter, Saturn, and Saturn's rings, a spectrum from a single night was sufficient. We only needed to look at the spatial resolution of the surface of the planet (or rings) to determine rotational velocity as we could differentiate between the two opposite sides of the planet (or rings). For example, see Figure 9 below for the image of Jupiter as it appeared over the spectrograph slit.

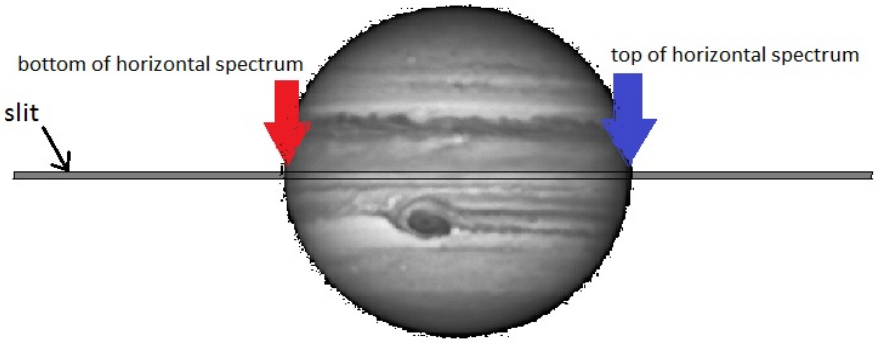

Figure 9: TV monitor view of Jupiter on the slit plate of the spectrograph

Both Jupiter and Saturn were positioned such that the slit passed through the equator of the planet (and plane of Saturn's rings). Note, however, that the spectrograph grating then rotates the spectrum by 90° such that the vertical displacement (y axis) of the spectrum represents the horizontal displacement of the slit (i.e., along the equator), as shown in Figure 10.

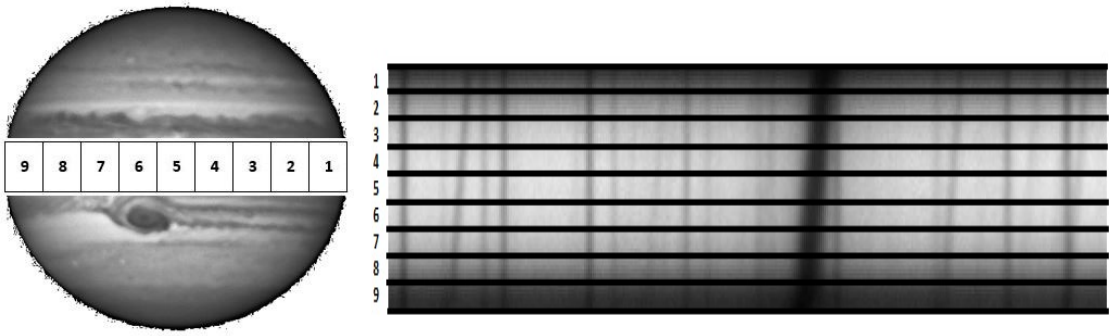

Figure 10: Binning Regions shown for Jupiter, horizontal "longitude" bins approximated on the TV monitor (left) versus the same bins aligned vertically on the actual spectrum (right).

Thus, when we consider a vertically displaced, horizontal binning region on our spectrum image, it represents a spectrum from a distinct longitude (horizontal region) along the equator of Jupiter. We used nine such bins for Jupiter and Saturn to look at the wavelength shift (red versus blue) with longitude in this way. We took only the binning regions at the very top and bottom of each spectrum for Saturn and Jupiter in order to calculate $\Delta\lambda_{obs}$ for equation (5) to determine their rotational velocities. For Io and Callisto, we did not take binning regions near the top and bottom of their spectra because we only wanted to measure their orbital velocities, not their rotational velocities. Hence, we took a single binning region that was in the middle of each spectrum to minimize the rotational velocity component, however small, of the moon.

As previously discussed in the methodology section, we needed to make a barycentric correction for Io and Callisto due to Earth's motion. The script we found online via the Astropy community allowed us to calculate a velocity correction value in km/s which was then used in BASS to apply to the spectra. For the Astropy script, we had to input the Coordinated Universal Time (UTC) date of observation along with the right ascension and declination of the object around the time of observation. These values were obtained via the Jupiter Ephemeris Generator 2.6. Once we obtained the velocity correction, BASS used this value along with the linear dispersion to create a one-dimensional spectral profile of our binning region, producing another line on the graph that had a discernible shift from the original spectrum. Thus, this correction allowed our $\Delta\lambda_{obs}$ to be more precise as the moon observations were separated by several weeks in time.

Note, all of the binning regions considered were approximately 3 pixels tall be-

cause we wanted the least amount of averaging over the possible slant of the hydrogen alpha spectral line.

5.2 Results

In order to calculate the $\Delta\lambda_{obs}$ term for equation (5), we needed to find the wavelength value of the center of the hydrogen alpha line. We used the Measurement Tool in BASS to fit the line profile and find the line center of the hydrogen alpha line. BASS reported the position with a precision of a tenth of a pixel, thus we take the measurement error to be ± 0.1 pixel. We repeated this process for each spectral binning region on our line graphs. Once the pixel values for the center of each hydrogen alpha line were determined, the respective pixel differences were multiplied by the linear dispersion (0.114 Å/pixel) to convert the difference into $\Delta\lambda_{obs}$. For the measurement error value of ± 0.1 pixel, $\Delta\lambda_{obs}$ becomes $\pm .01$ Å and equation (5) yields an error in the velocity values of ± 0.5 km/s. In Table 2, Δpx is listed for each object along with its associated $\Delta\lambda_{obs}$ and radial velocity from equation (5). In Figure 11, we have examples of the pixel line graphs that were used for locating the minima of the hydrogen alpha line.

Table 2: Radial Velocities for the Objects in the Solar System

Object	$\Delta px \pm .1px$	$\Delta\lambda_{obs} \pm .01$Å	$V_r \pm .5(km/s)$	Actual (km/s)
IO	13	1.48	16.9	17.3
Callisto	5	0.57	6.5	8.2
Saturn	7.2	0.82	9.4	9.9
Jupiter	9.6	1.09	12.5	12.6
Saturn's Rings	15.9	1.81	20.7	$\sim$18 (B ring)

The velocity determination for Saturn's rings is complicated by the Keplerian orbits and varying albedo of the ring particles. We did not attempt to make any corrections for this complicated scenario. Instead, we note the light from the B ring should dominant overall. Thus, we have noted its velocity as the actual value in Table 2.

In addition to the velocity determinations in Table 2, we wanted to visually showcase the Doppler shift of the hydrogen alpha line. The spectral line plots for each of the nine binning regions from Figure 10 for Jupiter and Saturn were exported to .xls files from BASS. The files were imported into Microsoft Excel and equation (5) was applied to convert the wavelength values into velocity values for the x-axis. The relative intensity on the y-axis was then artificially offset for each bin to allow

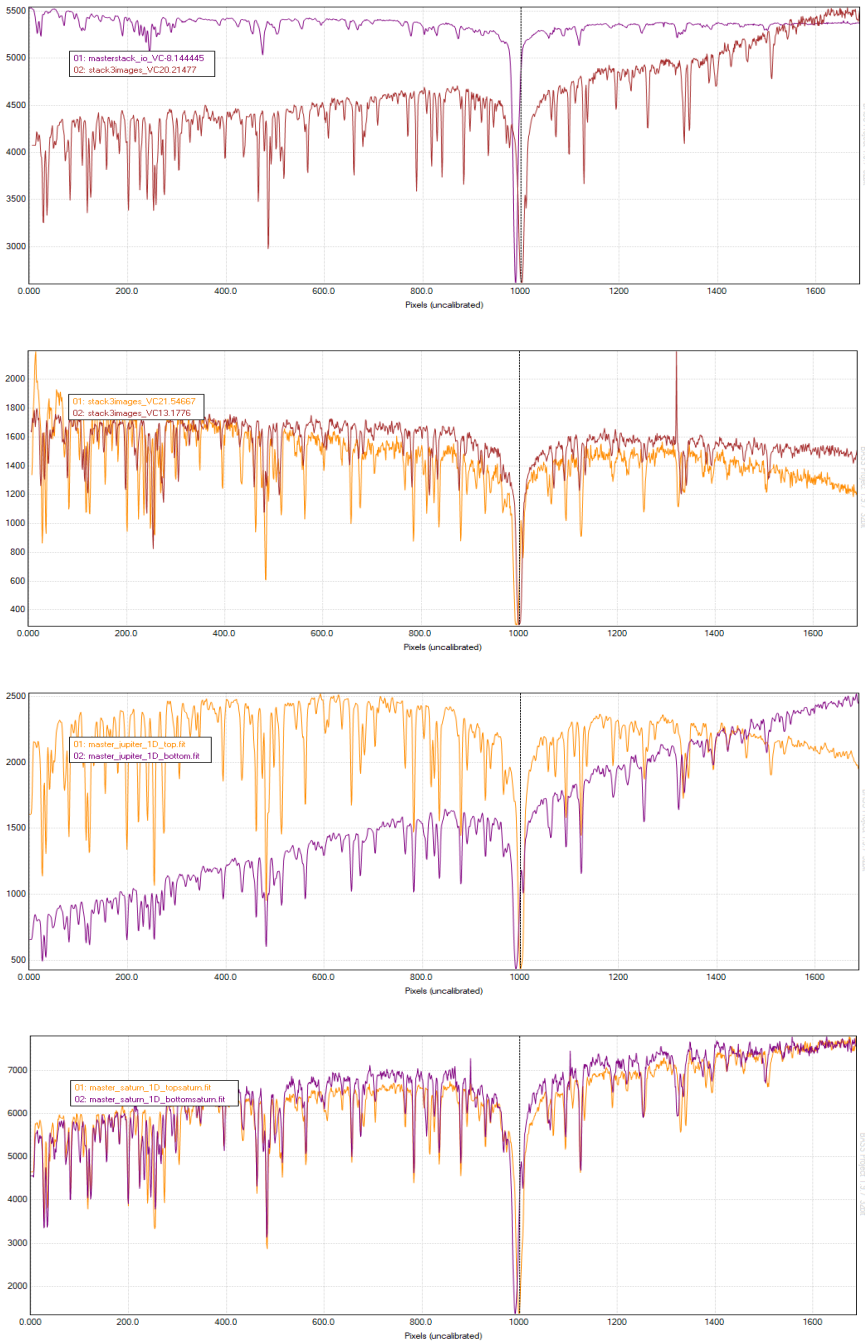

Figure 11: One dimensional line spectra produced by the BASS program. From top to bottom; Io, Callisto, Jupiter, Saturn.

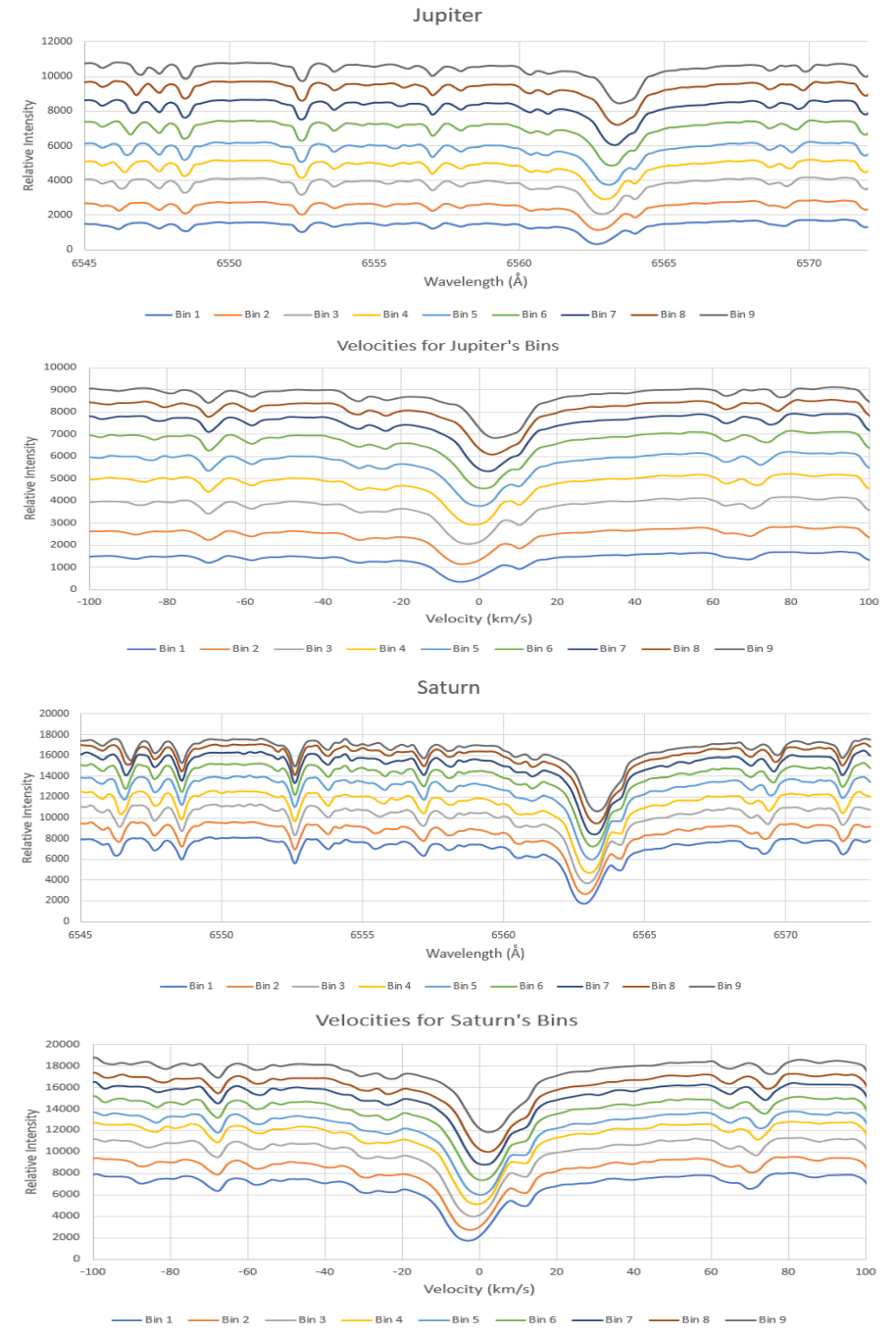

Figure 12: Wavelength and velocity plots of the nine binning regions across the disk of Jupiter and Saturn showing the position shift of the H-alpha absorption line.

all bins to be plotted on the same graph with a vertical offset. The result can be seen in Figure 12. Again, note that vertical offsets were applied to the intensity values to make the bins more discernible so ignore any perceived amplitude differences in the spectra. However, the H-alpha line itself does begin to overlap a telluric line at longer wavelength which does distort its most red shifted plot. We also note that a small fixed velocity correction was applied to adjust the "zero" velocity position to align more with the center of the nine bands. From Figure 12, we can see a velocity value of practically zero for the center most bin along the central meridian of Jupiter and Saturn, which is bin 5. Recall from Figure 10 that our binning regions run vertically from side to side on the planets. Therefore, this zero velocity value of the center region makes sense because there is minimal Doppler Shift in the radial velocity since the rotational velocity is almost entirely perpendicular to our line of sight.

5.3 Error

With the exception of Callisto and Saturn's rings, the results of our calculations are reasonably close to the known values for our objects' velocities. The BASS program measurement error of ± 0.1 pixel is likely to be too optimistic. A more realistic assessment is that the line centers can be determined to the nearest whole pixel. The use of equation (5) is applied to an error of 1 pixel in the line position, yielding a velocity error on the order of 1.0-1.5 km/s, which is a more appropriate indication of the uncertainty in the measurements. Although we have described the measurement error associated with $\Delta\lambda_{obs}$, there are additional sources of error involved. The timing of the maximum elongations for Io and Callisto was estimated and a window of roughly thirty minutes to an hour was needed for the observations, thus leaving ample room for the object to pass its true elongation point. This estimation of maximum elongation would have been less significant had we observed our objects for more nights (i.e. multiple nights of observation at each point of maximum elongation). However, we were only able to observe one point for one night in each pair of spectra for Io and Callisto. In turn, this would allow the averaging of multiple velocity calculations, hence improving the results. Another source of error came from the spatial averaging from the binning regions on our spectra, causing spatial averaging to the Doppler Shift. The overall effect of this would be to dilute the measured radial velocities resulting in values smaller than the actual maximum. Indeed our measured velocities are all smaller than the known values. This would be especially significant for Saturn's rings (which have the largest error) as the binning region spanned the width of the rings whose particles exhibit Keplerian rotation. The ring plane had a

sizeable inclination, and the region also spanned an appreciable arc of the circular ring plane.

6 Summary

The goal of this work was to accurately determine the orbital and rotational velocities of various objects in the solar system. As a whole, the procedure, instrumentation, and analysis proved to be adequate for determining such quantities through the radial velocity methodology. Thus, one could apply this work to other projects that involve measuring radial velocities of objects in the solar system, and to bright stellar objects in the space beyond. This project substantiated the capabilities of the equipment at the Harry D. Powell Observatory to perform astronomical spectroscopy. Future undergraduate students now have the opportunity to include such work as part of their undergraduate studies in observational astronomy at ETSU.

References

[1] Dingle, H. (1960). The Doppler Effect and the Foundations of Physics (I). *The British Journal for the Philosophy of Science, 11*(41), 11-31. Retrieved April 12, 2020, from www.jstor.org/stable/685816

[2] Showalter, Mark. (2016). *Jupiter Ephemeris Generator 2.6*, https://pds-rings.seti.org/tools/ephem2jup.html. Accessed on August-October 2019.

[3] Wilson, R. (1997). Ancient Astronomy. In *Astronomy through the Ages: The Story of the Human Attempt to Understand the Universe* (pp. 7-22). Princeton, New Jersey: Princeton University Press. doi:10.2307/j.ctv3hh4q3.6

[4] Evans, R. (2013). Retrieved from https://thecuriousastronomer.wordpress.com/2013/07/09/three-types-of-spectrums-spectra/

[5] Newton, Isaac. (1704). *Opticks: or, A treatise of the reflexions, refractions, inflexions and colours of light. Also two treatises of the species and magnitude of curvilinear figures* London, Printed for S. Smith, and B

[6] (2015, January 16). Frequency and Energy. Retrieved from https://spark.iop.org/frequency-and-energy on February 18, 2020

[7] Palma, Christopher. (2018) Stellar Velocities. Retrieved from https://www.e-education.psu.edu/astro801/content/

[8] Rodes, L. (1919). ON THE RELATION OF THE DOPPLER EFFECT TO KIRCHHOFF'S LAW. *Publications of the Astronomical Society of the Pacific, 31*(180), 91–102. Retrieved from www.jstor.org/stable/40693146

[9] Astrobodger. [Basic Astronomical Spectroscopy Software]. (2017). Version 1.9.7. Retrieved from http://customizedsynergy.com